Absence of Herpes Virus Entry Mediator (HVEM) Increases Bone Mass by Attenuating Receptor Activator of Nuclear Factor-κB ligand (RANKL)-Induced Osteoclastogenesis

Woon-Ki Kim,* Ok-Joo Sul,* Eun-Kyung Choi, Mi-Hyun Lee, Choon-Soo Jeong, Hyun-Ju Kim, Shin-Yoon Kim, Jae-Hee Suh, Rina Yu, and Hye-Seon Choi

Department of Biological Sciences (W.-K.K., O.-J.S., E.-K.C., M-H.L., C.-S.J., H.-S.C.), University of Ulsan, Ulsan 680–749, Korea; Skeletal Diseases Genome Research Center (H.-J.K., S.-Y.K.), School of Medicine, Kyungpook National University, Daegu 700–412, Korea; Department of Pathology (J.-H.S.), Ulsan University Hospital, Ulsan 682–714, Korea; and Department of Food Sciences (R.Y.), University of Ulsan, Ulsan 680–749, Korea

Herpes virus entry mediator (HVEM), which is constitutively expressed at a high level on myeloid lineage cells, is also expressed on bone marrow-derived macrophages, suggesting that it may play a role in bone metabolism by affecting osteoclasts (OC) derived from bone marrow-derived macrophages. To address this question, we evaluated bone mass by micro-computed tomography and the number and activity of OC by tartrate-resistant acid phosphatase (TRAP) and pit formation on dentine slices, comparing HVEM-knockout mice with wild-type mice. The absence of HVEM led to a higher bone mass and to decreased levels of serum collagen type I fragments and serum TRACP5b *in vivo*. *In vitro* HVEM deficiency resulted in a reduced number and activity of OC and an impaired receptor activator of nuclear factor-κB ligand signaling through reduced activation of nuclear factor-κB and of nuclear factor of activated T-cells cytoplasmic 1. Exogenous soluble HVEM decreased expression of TRAP, whereas soluble LIGHT (a ligand of HVEM) increased it, indicating the occurrence of a positive signaling through HVEM during osteoclastogenesis. Our findings indicate that HVEM regulates bone remodeling via action on OC. The higher bone mass in the femurs of HVEM-knockout mice could be, at least in part, due to attenuated osteoclastogenesis and bone resorption resulting from decreased receptor activator of nuclear factor-κB ligand signaling in the OC. **(*Endocrinology* 153: 4808–4817, 2012)**

Bone is a dynamic tissue that undergoes remodeling as a consequence of the activities of osteoclasts (OC) and osteoblasts. OC are giant multinucleated cells that are primarily responsible for bone destruction (1). Two key molecules have been identified to be promoting osteoclastogenesis. These necessary and sufficient factors are produced by bone marrow stromal cells. They are macrophage colony-stimulating factor (M-CSF) and receptor activator of nuclear factor-κB ligand (RANKL), a member of the TNF family (1, 2). Binding of RANKL to its receptor, RANK, recruits TNF receptor-associated factor 6 (TRAF6) and activates downstream signaling pathways such as nuclear factor-κB (NF-κB) and nuclear factor of activated T cells, cytoplasmic 1 (or NFAT2) that are essential for OC differentiation (3–5). Activated transcription factors initiate expression of target genes including tartrate-resistant acid phosphatase (TRAP) and cathepsin K (4, 5). OC are highly regulated cells that act in an autocrine fashion to produce modulating factors that promote their own formation and activity (1).

ISSN Print 0013-7227 ISSN Online 1945-7170
Printed in U.S.A.

doi: 10.1210/en.2012-1079 Received January 20, 2012. Accepted July 12, 2012.
First Published Online August 3, 2012

* W.-K.K. and O.-J.S. contributed equally to this work.

Abbreviations: Ab, Antibody; BMC, bone mineral content; BMD, bone mineral density; BMM, bone marrow-derived macrophage; $[Ca^{2+}]i$, intracellular concentration of Ca^{2+}; μCT, micro-computed tomography; DCFH-DA, 2′,7′-dichlorofluorescein diacetate; HVEM, Herpes virus entry mediator; KO, knockout; M-CSF, macrophage-colony stimulating factor; MNC, multinucleated cells; NFAT2, nuclear factor of activated T cells cytoplasm 1; NF-κB, nuclear factor-κB; OC, osteoclast; qPCR, quantitative PCR; ROS, reactive oxygen species; RANKL, receptor activator of nuclear factor-κB ligand; sHVEM, soluble HVEM; sLIGHT, soluble LIGHT; TNFR, TNF receptor; TRAF6, TNFR-associated factor 6; TRAP, tartrate-resistant acid phosphatase; TUNEL, terminal deoxynucleotide transferase-mediated dUTP nick end labeling WT, wild type.

In addition to RANKL/RANK, several TNF receptors (TNFR)/TNF ligand interactions that primarily affect the immune system influence the differentiation and function of OC (6–10), indicating that the two systems are closely related. Herpes virus entry mediator (HVEM) is a TNFR family member like RANK and was originally identified as the receptor for Herpes simplex virus 1 (11). HVEM transmits a signal that leads to activation of NF-κB (12), a transcriptional regulator of inflammatory genes. LIGHT, a TNF family member, interacts with HVEM as well as the lymphotoxin β receptor and the decoy receptor DcR3/TR6 (13). HVEM and LIGHT are expressed prominently on lymphoid cells and myeloid lineage cells with a wide tissue distribution (13). Cross-linking of LIGHT to HVEM stimulates T cells and accelerates proliferation and cytokine production (14). In addition to acting as a T cell costimulator, the HVEM/LIGHT interaction is involved in the maturation of dendritic cells (15) and the bactericidal activity of monocytes (16), which implies that HVEM also plays a role in myeloid cells. The strong and constitutive expression of HVEM in myeloid lineage cells, which are also OC precursors, suggests that HVEM influences bone metabolism by acting on OC.

In the present work we have attempted to clarify the role of HVEM in OC and its effect on the skeletal phenotype using HVEM-deficient mice.

Materials and Methods

Reagents and antibodies

Recombinant mouse M-CSF, RANKL, HVEM, and LIGHT were obtained from R&D Systems, Inc. (Minneapolis, MN). Monoclonal antibody (Ab) against HVEM was raised against an HVEM-Fc fusion protein and was shown to block T cell proliferation upon stimulation with CD3 and the soluble form of LIGHT (17).

OC formation, bone resorption, and bone measurement

Bone marrow cells (typically three mice per preparation) were isolated from 4- to 5-wk-old male HVEM$^{+/+}$ wild-type (WT) and HVEM$^{-/-}$ [HVEM-knockout (KO)] mice on a background of C57BL/6J mice purchased from The Jackson Laboratory (Bar Harbor, ME) and provided by the University of Ulsan Immunomodulation Research Center (IRC). HVEM-KO mice were made as described previously (17). The genotypes of the offspring were determined by Southern blot analysis of DNA from tail biopsies. All mice were housed in the specific pathogen-free animal facility of the IRC and were handled in accordance with the guidelines of the Institutional Animal Care and Use Committee of the IRC. Standards were approved by the committee (2008-033). Femurs and tibias were removed aseptically and adherent soft tissue was removed. The bone ends were cut, and the marrow cavity was flushed out with α-MEM from one end of the bone using a sterile 21-gauge needle, after which the marrow was agitated using a Pasteur pipette to obtain a cell suspension. The resulting bone marrow suspension was washed twice and incubated on plates with M-CSF (20 ng/ml) for 16 h. Nonadherent cells were then harvested, layered on a Ficoll-hypaque gradient for collecting cells at the interface, and cultured for 2 more days as described previously (18), at which time large populations of adherent monocyte/macrophage-like cells had formed on the bottom of the culture plates. The small number of nonadherent cells was removed by washing the dishes with PBS, and the remaining adherent cells [bone marrow-derived macrophages (BMM)] were harvested and seeded on plates. The adherent cells were analyzed by fluorescence-activated cell sorter (FACS) and found to be negative for CD3 and CD45R and positive for CD11b and F4/80. The absence of contaminating stromal cells was confirmed by a lack of growth without the addition of M-CSF. Additional medium containing M-CSF and RANKL (40 ng/ml) was added, and the medium was replaced on d 3. After incubation for the indicated times, the cells were fixed in 10% formalin for 10 min and stained for TRAP as previously described (1). Numbers of TRAP-positive multinucleated cells (MNC) (three or more nuclei) were determined

OC were further characterized by assessing their ability to form pits on dentine slices, as previously described (19). Mature OC were generated by incubation with M-CSF and RANKL for 5 d and harvested as previously described (20). The cells obtained (2000 cells) were seeded on dentine slices and incubated for 1 d with M-CSF and RANKL. The slices were cleaned by ultrasonication in 1 M NH_4OH to remove adherent cells, then stained with Mayer's hematoxylin (Sigma Chemical Co., St. Louis, MO) to visualize resorption pits.

Micro-computed tomography (μCT) scanning was performed with a GE eXplore Locus SP system (Locus SP; GE Healthcare Co., Piscataway, NJ) as previously described (21). For three-dimensional histomorphometry and visualization of long bone structure, the femurs of 10-wk-old female mice were scanned with a high-resolution μCT imaging system set to a 0.008-mm effective detector pixel size. The software for the three-dimensional microstructure analysis was provided by Explore MicroView 2.2. The following bone remodeling markers were measured according to the manufacturer's directions (Immunodiagnostic Systems Inc., Jena, Germany): serum collagen-type I fragments (CTX-1) by RatLaps enzyme immunoassay, serum TRACP5b by solid phase immune-fixed enzyme activity assay, and N-terminal propeptide of type I procollagen (PINP) by competitive enzyme immunoassay. For *in vivo* TRAP-positive OC analysis, mouse femurs were excised, cleaned of soft tissue, and decalcified in EDTA. Representative histological sections of distal femoral metaphysis of WT and HVEM-KO mice were stained for TRAP to identify OC that were decreased in the mutant (original magnification $\times$ 200). *In vivo* apoptosis was measured using a TUNEL (terminal deoxynucleotide transferase-mediated dUTP nick end labeling) assay according to the manufacturer's instructions (ApopTag Peroxidase In Situ Detection kit; Chemicon, Temecula, CA). Bone histomorphometry was measured using Image Pro Plus 3.0 software (Media Cybernetics, Silver Spring, MD).

Quantitative PCR (qPCR)

Total RNA from BMM incubated with M-CSF and RANKL for the indicated time period was extracted using Trisol solution

(Life Technologies, Inc., Gaithersburg, MD), and reverse transcribed with oligo-dT and Superscript I (Invitrogen, Carlsbad, CA). qPCR was carried out using SYBR Green 1 Taq polymerase (QIAGEN, Hilden, Germany) and appropriate primers on a DNA Engine Opticon Continuous Fluorescence Detection System (MJ Research Inc., Waltham, MA). The specificity of each primer pair was confirmed by melting curve analysis and agarose-gel electrophoresis. The housekeeping glyceraldehyde-3-phosphate dehydrogenase gene was amplified in parallel with the genes of interest. Relative copy numbers compared with glyceraldehyde-3-phosphate dehydrogenase were calculated using $2^{-\Delta\Delta Ct}$. Primer sequences used were described in Supplemental Table 1 published on The Endocrine Society's Journals' Online web site at http://endo.endojournals.org.

Apoptosis assay

OC apoptosis was detected by annexin V staining. OC derived from BMM stimulated with RANKL for 4 d were washed and incubated with or without cytokines for 18 h. For annexin V staining, the cells were harvested as previously described (20) and transferred to FACS tubes. After washing, cells were incubated with annexin V fluorescein isothiocyanate (BD Biosciences, Palo Alto, CA) in binding buffer [10 mM HEPES/NaOH (pH 7.4), 140 mM NaCl, 2.5 mM $CaCl_2$] for 15 min and immediately analyzed with a FACSCalibur (Becton Dickinson, Franklin Lakes, NJ).

EMSA

Biotinylated double-stranded oligonucleotides were synthesized by Bioneer Co. (Daejeon, Korea): NF-κB, 5′-agttgaggggac tttcccaggc-3′; NF-κB-mutant, 5′-agttgaggcgactttcccaggc-3′; NF-Y, 5′-agaccgtacgtgattggttaatctctt-3′. Nuclear extracts were prepared from BMM cells stimulated with RANKL (40 ng/ml) using NE-PER nuclear and cytoplasmic extraction reagents (Pierce Chemical Co., Rockford, IL) according to the manufacturer's manual. Binding reactions were carried out for 20 min at room temperature in the presence of 50 ng/ml polydeoxyinosinic deoxycytidylic acid, 0.05% Nonidet P-40, 5 mM $MgCl_2$, 10 mM EDTA, and 2.5% glycerol in 1 × binding buffer using 20 fmol of biotin-end-labeled target DNA and 3 μg of nuclear extract according to the manufacturer's manual (LightShift Chemiluminescent EMSA kit; Pierce). Samples were loaded onto native 6% polyacrylamide gels preelectrophoresed for 60 min in 0.5 × Tris borate/EDTA and electrophoresed at 100 V before being transferred onto a positively charged nylon membrane (Hybond-N+) in 0.5 × Tris borate/EDTA at 100 V for 30 min. Transferred DNA were cross-linked to the membrane at 10 mJ/cm^2 and detected using horseradish peroxidase-conjugated streptavidin.

Fractionation and Western blot analysis

Cultured cells were harvested after washing with ice-cold PBS and then lysed in extraction buffer (50 mM Tris-HCl, pH 8.0; 150 mM NaCl; 1 mM EDTA; 0.5% Nonidet P-40; 0.01% protease inhibitor mixture). Cells were fractionated using Nuclear and Cytoplasmic Extraction reagents (Pierce) according to the manufacturer's protocol. Cytoplasmic and nuclear extracts were subjected to SDS-PAGE and Western blotting. The primary Ab used were Ab against NFAT2 and lamin B (Santa Cruz Biotechnology, Inc., Santa Cruz, CA) and β-actin (Sigma). Horseradish peroxidase -conjugated secondary Ab (BD Biosciences) was used as the probe.

Intracellular reactive oxygen species (ROS) detection

The intracellular formation of ROS was detected using the fluorescence probe 2′,7′-dichlorofluorescein diacetate (DCFH-DA) (Molecular Probes, Inc., Eugene, OR). After BMM were cultured under the different experimental conditions for 48 h, the cells were harvested, suspended in PBS, loaded with DCFH-DA, and incubated at 37 C for 30 min. The measurement of intracellular ROS was performed using flow cytometry with a FACSCalibur.

Measurement of intracellular concentration of Ca^{2+} ($[Ca^{2+}]i$)

BMM were incubated with RANKL and M-CSF for 48 h. For $[Ca^{2+}]i$ measurement, cells were incubated with 5 μM fluo-4 AM, 5 μM Fura Red AM, and 0.05% pluronic F127 for 30 min in serum-free DMEM as previously described (5). Cells were further incubated with M-CSF for 20 min and analyzed using a confocal microscope (FV1000; Olympus, Tokyo, Japan). To estimate $[Ca^{2+}]i$ in a single cell, the ratio of the fluorescence intensity of fluo-4 to Fura Red was calculated. The increase in the ratio from the basal level was divided by the maximum ratio increase obtained by adding 10 μM ionomycin and was expressed as the % maximum ratio increase. For measurement of total $[Ca^{2+}]i$, BMM cultured with RANKL and M-CSF for 48 h were loaded with fluo-4 at 37 C for 30 min, further incubated at room temperature for an additional 30 min, and analyzed with an excitation/emission filter pair (488/530 nm).

Statistical analysis

All values are expressed as means ± SEM. Statistical significance was determined by Student's *t* test. $P < 0.05$ was considered statistically significant.

Results

HVEM increases OC number and activity *in vitro*

HVEM is highly expressed on monocytes and macrophages (13), the precursors of which share characteristics with OC. BMM were exposed to RANKL to determine whether HVEM expression was regulated during osteoclastogenesis. HVEM was constitutively expressed in BMM and was significantly up-regulated after 8 h of exposure to RANKL but decreased afterward (Fig. 1A). To evaluate whether HVEM influenced osteoclastogenesis, we determined OC formation in cultures of BMM isolated from WT and HVEM-KO mice. In the presence of the two osteogenic cytokines, M-CSF and RANKL, maximal OC formation occurred after 3 d. The extent of OC formation in the HVEM-KO BMM was 37% lower than in the WT BMM as measured by counting TRAP-positive MNC (Fig. 1, B and C). Furthermore, the absence of HVEM reduced

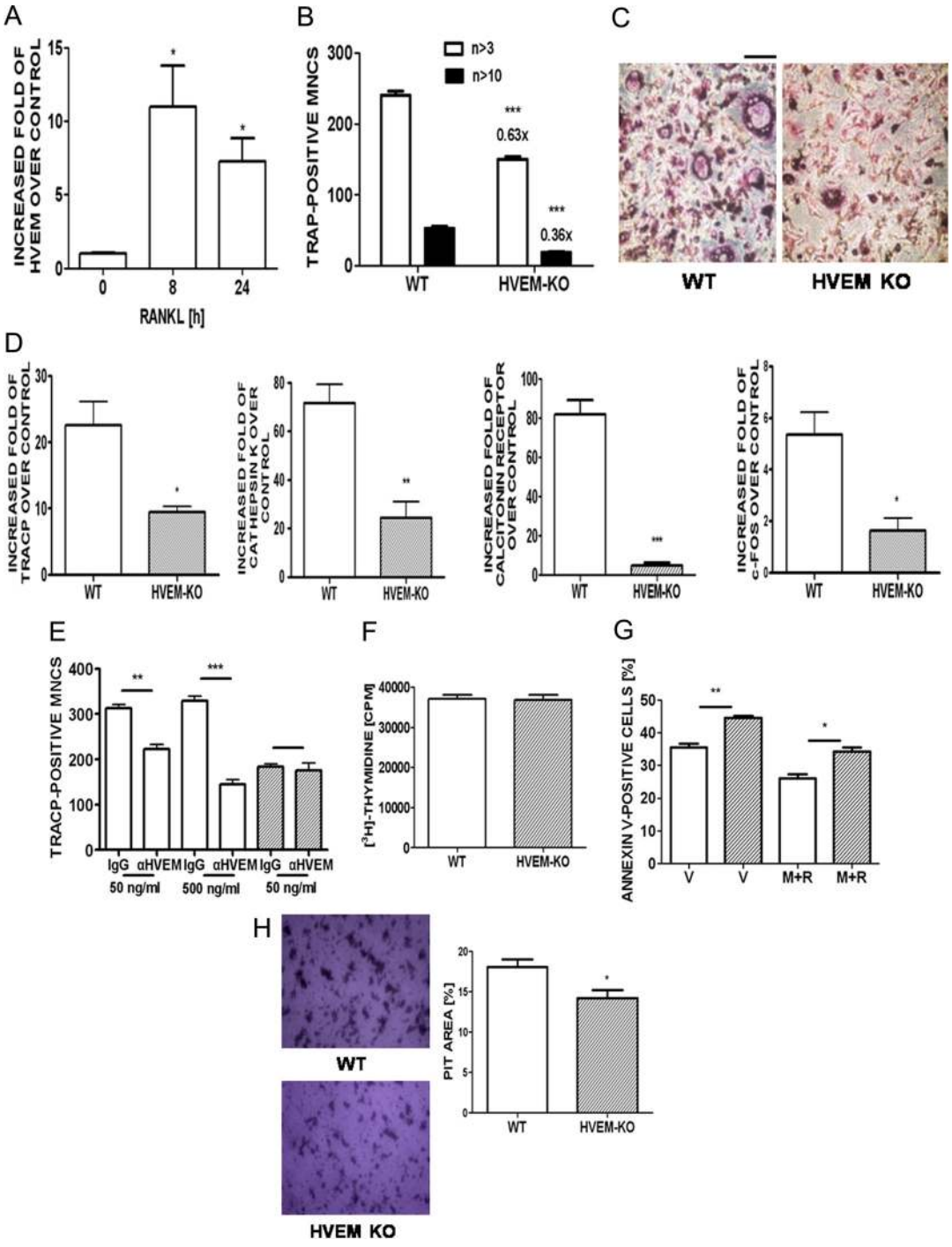

FIG. 1. Reduced number and activity of OC in the absence of HVEM. A and D, BMM were stimulated with RANKL (40 ng/ml) and M-CSF (20 ng/ml) for 8, 24 (A), and 48 h (D), and total RNA was extracted and subjected to qPCR analysis. The expression level before RANKL treatment was set at 1. *, $P < 0.05$ compared with the level before RANKL treatment (A). *, $P < 0.05$; **, $P < 0.01$; ***, $P < 0.001$ compared with WT cells (D). B, BMM from WT and HVEM-KO mice were incubated with M-CSF and RANKL. After 3 d, the cells were fixed and the number of TRAP-positive MNC per well was scored (n > 3, OC having >3 nuclei; n > 10, OC having >10 nuclei). ***, $P < 0.001$ compared with WT cells. C, Representative photos of B; *scale bar*; 200 μm. E, BMM were stimulated with RANKL in the presence of control IgG (IgG) or anti-HVEM Ab (αHVEM) and M-CSF for 3 d. **, $P < 0.01$; ***, $P < 0.001$ compared with control IgG-treated cells. There was no significant difference between treatments of control IgG and anti-HVEM Ab in HVEM-KO cells. F, BMM were incubated with M-CSF for 1 d. For the final 18 h of culture, they received 1 μCi/well [^{3}H]thymidine (NEN Life Science Products, Boston, MA). Cellular DNA was harvested and counted by liquid scintillation spectroscopy. There was no significant difference between WT BMM and HVEM-KO BMM. G, Mature OC were washed, reincubated with vehicle (V) or M-CSF and RANKL (M+R) for 18 h, and apoptotic cells were stained with annexin V fluorescein isothiocyanate. *, $P < 0.05$; **, $P < 0.01$ compared with WT cells. H, Mature OC were incubated on whole dentine slices in the presence of M-CSF and RANKL for 1 d, and the slices were stained with Mayer's hematoxylin. Representative photos of the resorption pits formed by WT OC and HVEM-KO OC are shown. The areas of the resorption pits were measured with ImageJ 1.37v. *, $P < 0.05$ compared with WT cells. WT cells, *open bars*; HVEM-KO cells, *diagonally lined bars* (D–H). Similar results were obtained in three independent experiments.

OC with more than 10 nuclei by a greater degree, compared with those having more than three nuclei (37% *vs.* 64%). Consistent with this result, after 48 h of RANKL stimulation, transcripts of TRAP, cathepsin K, calcitonin receptor, and c-Fos were significantly lower in the OC from HVEM-KO mice than in those from WT mice (Fig. 1D). To confirm that the decreased OC formation observed in HVEM-KO BMM was a direct effect of HVEM deficiency, we incubated WT BMM with anti-HVEM Ab to block HVEM. As anticipated, neutralization of HVEM significantly reduced osteoclastogenesis in WT BMM, with no effect on HVEM-KO BMM (Fig. 1E). To assess whether the decreased OC formation was due to retarded cell growth in the absence of HVEM, we examined the proliferation of BMM upon stimulation with M-CSF. There was no significant difference in proliferation between BMM from WT and HVEM-KO mice (Fig. 1F). We also assessed whether the decreased OC formation in the absence of HVEM was due to decreased OC survival. To examine whether decreased OC survival was caused by an increased apoptotic effect, binding to annexin V was determined. A significant increase in annexin V-positive cells was observed with HVEM-KO cells after withdrawal or restimulation of M-CSF and RANKL compared with WT cells (Fig. 1G). Next, we assessed whether HVEM affected bone resorption. Mature OC from HVEM-KO mice gave rise to significantly fewer pits than did the same number of WT OC (Fig. 1H).

HVEM stimulates bone remodeling *in vivo*

The finding that constitutively expressed HVEM acted as a positive regulator in OC suggests a role of HVEM in bone loss *in vivo*. To determine whether our *in vitro* findings apply *in vivo*, we analyzed femur bones from HVEM-KO mice and their littermates by μCT. At 10 wk of age, no significant differences in body size and shape were observed between the HVEM-KO and WT mice (data not shown). μCT analysis of femurs revealed that loss of HVEM function led to higher bone mass in basal conditions (Fig. 2A). The bone mass increase in HVEM-KO mice was evaluated at the level of the secondary spongia of the distal femurs. HVEM-KO mice had elevated bone mineral densities (BMD), bone mineral content (BMC), and trabecular bone volume (BV/TV), and reduced trabecular separation (Tb.Sp.) (Fig. 2, B–G). The decreased bone resorption in HVEM-KO mice was confirmed by the reduced level of serum CTX-1 (Fig. 2H). A reduced number of OC was observed by lower serum TRACP5b in the absence of HVEM, compared with WT (Fig. 2I). In agreement with this, histological sections of the distal femur also showed a lower number of TRAP-positive OC in the absence of HVEM (Fig. 2J). To confirm that this decrease was due to the enhanced susceptibility of OC to apoptosis, *in vivo* TUNEL staining was performed. Contrary to our *in vitro* results, a lack of HVEM reduced the number of TUNEL-positive cells compared with WT *in vivo* (Fig. 2K). However, a serum marker of bone formation, PINP, was not significantly affected by the lack of HVEM (Fig. 2L).

HVEM regulates RANKL signaling by modulating NF-κB activation and NFAT2 induction

To gain molecular insights into the enhancing role of HVEM in osteoclastogenesis, we investigated the effect of HVEM deficiency on RANKL-induced signaling pathways. Because HVEM did not affect M-CSF-stimulated proliferation in BMM (Fig. 1F), we hypothesized that HVEM might mediate RANKL-regulated OC differentiation. Occupancy of RANK activates the key osteoclastogenesis transcription factors NF-κB and NFAT2 (4, 5). We first asked whether the absence of HVEM affected the activation of NF-κB induced by RANKL. RANKL stimulation of BMM induced NF-κB DNA binding activity (lane 3), whereas the absence of HVEM decreased this activity (lane 5) (Fig. 3A). The specificity of the binding activity was confirmed by competition assays using mutant competitor probes (lane 1).

Next, we showed that the exposure of BMM to RANKL increased transcript levels of NFAT2. The level of NFAT2 was significantly lower in the absence of HVEM when compared with WT cells (Fig. 3B). We examined the expression and cellular location of NFAT2 protein in RANKL-stimulated BMM undergoing differentiation. A reduced level of total NFAT2 protein was found in HVEM-KO cells (Fig. 3C, *lower panel*). RANKL stimulation strongly induced enrichment of NFAT2 in the nucleus region of WT OC, compared with HVEM-KO OC (Fig. 3C, *upper and middle panels*), suggesting that HVEM deficiency decreased nuclear localization of NFAT2 in OC. Because autoamplification of NFAT2 during OC formation is associated with RANKL-induced long-lasting ROS production (22) and $[Ca^{2+}]i$ oscillation (5), we evaluated whether the absence of HVEM also affected long-term ROS production and $[Ca^{2+}]i$ oscillation after exposure to RANKL. RANKL stimulation sustained an elevated level of ROS, which was maximal at 48 h exposure, compared with M-CSF stimulation in WT cells (Fig. 3D). HVEM deficiency reduced ROS levels induced by RANKL as well as M-CSF (Fig. 3D). As shown in Fig. 3E, total $[Ca^{2+}]i$ was also significantly attenuated in the absence of HVEM compared with WT cells upon RANKL stimulation. Furthermore, the degree of the $[Ca^{2+}]i$ oscillation response of each individual cell was also lower in the absence of HVEM (Fig. 3F).

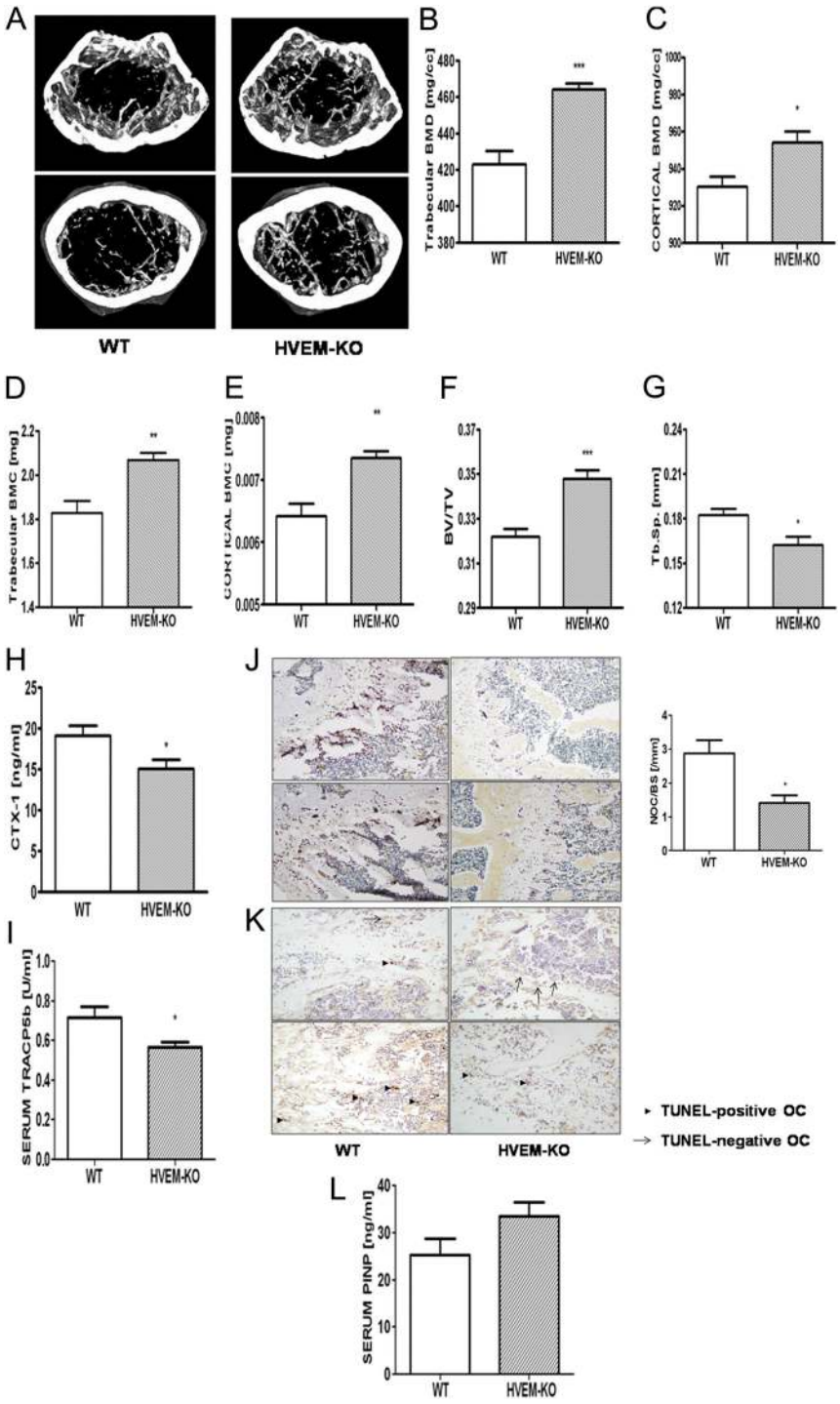

FIG. 2. Bone mass increases in the absence of HVEM. A, The μCT images in the *upper and lower panels* correspond to the regions 0.7 mm and 2.3 mm, respectively, from the growth plate of the distal femur. B–G, Trabecular BMD, cortical BMD, trabecular BMC, cortical BMC, trabecular bone volume (BV/TV), and distance between successive trabeculae (Tb.Sp) in the distal femurs of WT (*open bars*) and HVEM-KO (*diagonally lined bars*) mice were measured by μCT. H and I, OC activity and number were assessed by measuring serum CTX-1 (H) and serum TRACP5b (I), respectively. J and K, TRAP staining (J) and TUNNEL staining (K) of the histological section of the distal femur showed that the number of OC was reduced in the mutant (NOC/BS, OC number over total bone surface). *In vivo* TUNEL staining revealed more apoptotic OC-like cells in WT compared with the mutant. L, *In vivo* bone formation was measured by serum PINP. Data are expressed as means ± SEM. *, $P < 0.05$; **, $P < 0.01$; ***, $P < 0.001$ compared with WT mice.

Because activation of three members of the MAPK family, p38, ERK, and JNK, is important for RANKL-induced osteoclastogenesis, we examined whether the absence of HVEM also affected the activations of these MAPK. There was no significant difference in the phosphorylation of MAPK between WT and HVEM-KO cells upon RANKL stimulation (data not shown).

A signal through HVEM stimulates RANKL-induced OC formation

Because OC differentiation was reduced in the absence of HVEM or by blockade of HVEM by neutralizing Ab, an HVEM-mediated signal should be stimulatory for OC formation. To search for possible HVEM ligand candidates for increased OC formation, we examined the expression of LIGHT in BMM upon RANKL stimulation. LIGHT was also constitutively expressed in BMM, down-regulated after 8 h of RANKL exposure, and afterward returned to its original level (Fig. 4A). To assess whether LIGHT was required for the increased OC formation mediated by HVEM, we treated BMM with soluble LIGHT (sLIGHT) to stimulate HVEM and assessed RANKL-induced OC formation by measuring TRAP expression. sLIGHT increased osteoclastogenesis significantly in WT cells but had no effect on HVEM-KO cells (Fig. 4B), suggesting that sLIGHT transmits a signal inducing osteoclastogenesis. To confirm the effect of sLIGHT, we counted TRAP-positive MNC after stimulation with RANKL and sLIGHT for 3 d. As shown in Fig. 4C, we detected a similar pattern to that observed for TRAP transcript. The effect of sLIGHT on RANKL-stimulated ROS production also showed a similar pattern: WT cells generated elevated levels of ROS upon RANKL stimulation by sLIGHT, whereas HVEM-KO cells did not (Fig. 3D). We also investigated whether LIGHT alone induces OC formation, and, if so, whether it is independent of RANKL. As shown in Fig. 4D,

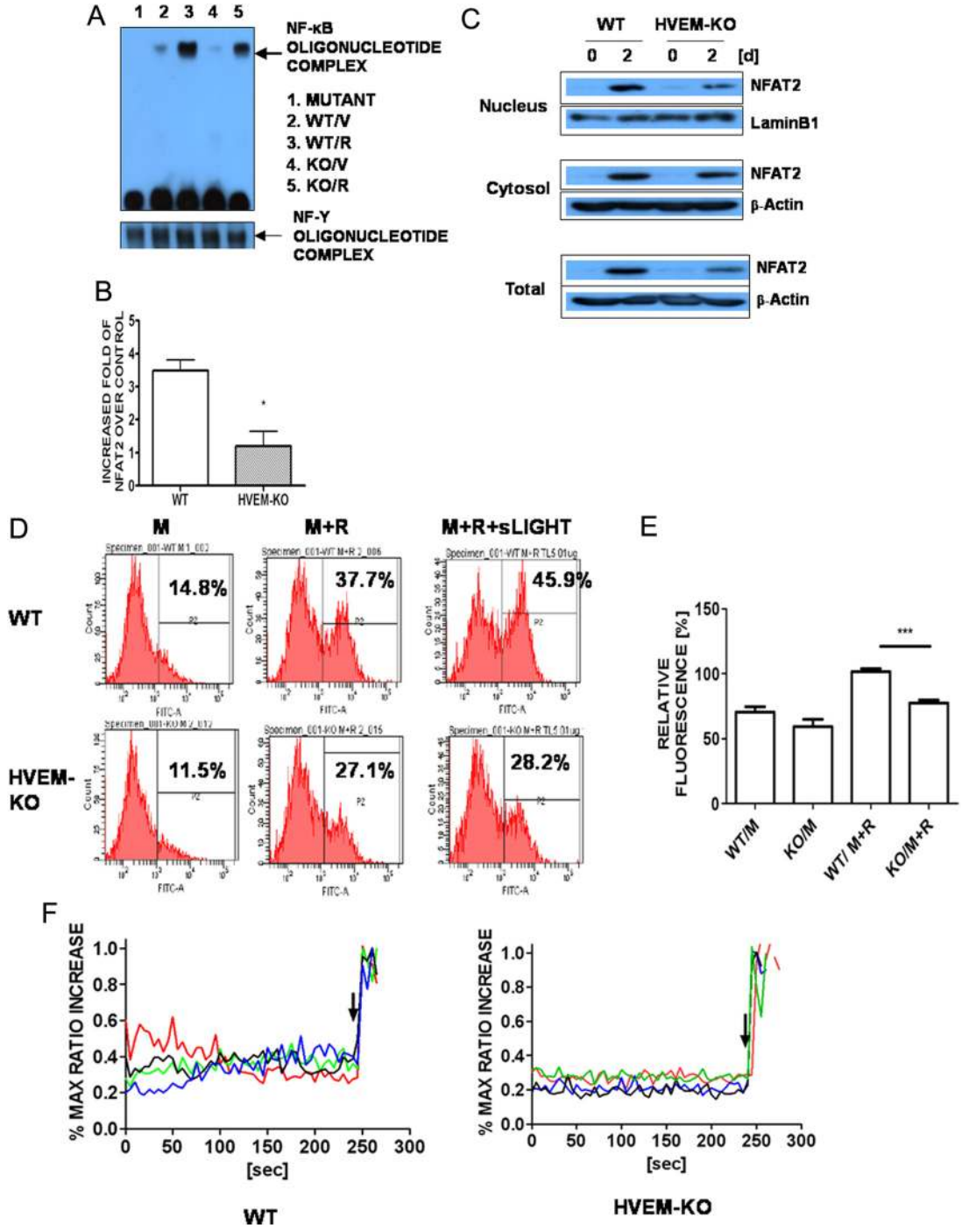

FIG. 3. Impaired RANKL signaling in OC in the absence of HVEM. A, BMM were stimulated with vehicle (V: lanes 2 and 4) or RANKL (100 ng/ml) (R: lanes 3 and 5) for 1 h. A variant NF-κB (lane 1) was used as a negative control. NF-Y DNA binding activity was measured as an internal control. B, BMM were stimulated with RANKL (40 ng/ml) and M-CSF (20 ng/ml) for 48 h, and total RNA was extracted and subjected to qPCR analysis. The expression level before RANKL treatment was set at 1. *, $P < 0.05$ compared with WT cells. WT cells, *open bar*; HVEM-KO cells, *oblique-lined bar*. C, BMM were cultured for 2 d in the presence of M-CSF and RANKL. Whole-cell extracts, cytoplasmic fractions, and nuclear fractions were harvested from cultured cells and subjected to Western blot analysis with specific Ab as indicated. Ab for β-actin and lamin B1 were used for the normalization of cytoplasmic and nuclear extracts, respectively. D, Intracellular levels of ROS upon stimulation with RANKL or RANKL+sLIGHT (0.1 μg/ml) in the presence of M-CSF for 48 h were determined in WT cells and HVEM-KO cells using DCFH-DA. ROS levels were quantified by flow cytometry. E and F, WT BMM and HVEM-KO BMM were cultured with M-CSF and RANKL for 48 h. Cells were loaded with fluo-4 AM for fluorescence (E). ***, $P < 0.001$ compared with WT cells. Cells were loaded with fluo-4 and Fura Red, and the ratio of fluorescence intensity of fluo-4 to Fura Red was estimated, and percent maximum ratio increase from the base line was plotted with an interval of 5 sec. Maximum ratio increase was obtained with the addition of 10 μM ionomycin at the end of each experiment, indicated by an *arrow*. Each line indicated a different cell in the same field (F). M, M-CSF; MAX, maximal; R, RANKL; KO, HVEM-KO.

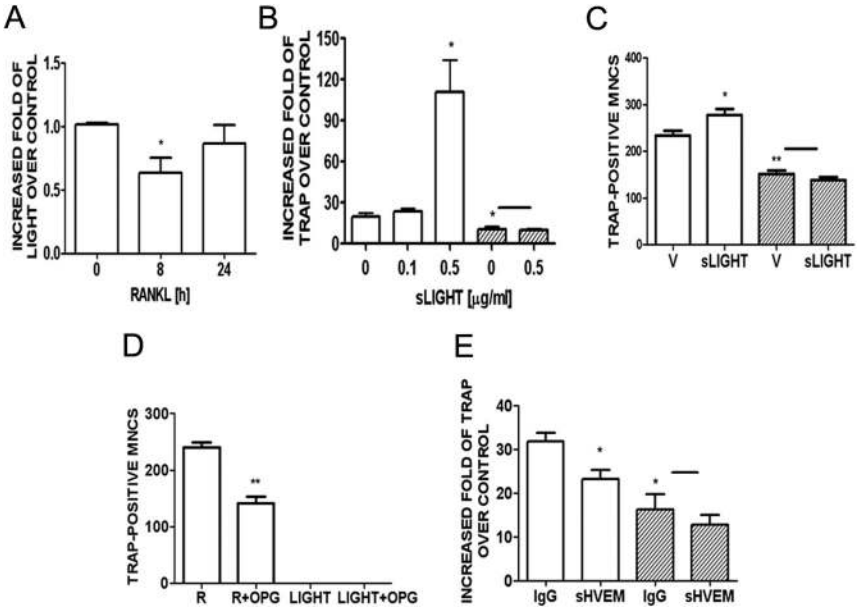

FIG. 4. A signal through HVEM increases OC formation. A, BMM were stimulated with RANKL and M-CSF for 8 and 24 h, and total RNA was extracted and subjected to qPCR analysis for LIGHT. The expression level before RANKL treatment was set at 1. *, $P < 0.05$ compared with the level before RANKL treatment. B and C, WT BMM and HVEM-KO BMM were stimulated with RANKL in the presence of vehicle or sLIGHT for 48 h for qPCR (B), and 72 h for TRAP staining (sLIGHT, 0.2 μg/ml) (C). Total RNA was extracted and subjected to qPCR analysis for TRAP. The expression level before RANKL treatment was set at 1. *, $P < 0.05$; **, $P < 0.01$ compared with vehicle-treated WT cells. There was no significant difference between sLIGHT treatment and vehicle (V) in HVEM-KO cells. D, M-CSF-treated BMM were stimulated with RANKL (R) or LIGHT in the presence or absence of osteoprotegerin (OPG) (50 ng/ml) for 72 h for TRAP-staining. **, $P < 0.01$ compared with RANKL-treated cells. E, BMM were stimulated with RANKL in the presence of control IgG or sHVEM (0.2 μg/ml) for 48 h. *, $P < 0.05$ compared with control IgG-treated WT cells. There was no significant difference between sHVEM treatment and vehicle in HVEM-KO cells. WT cells, *open bars*; HVEM-KO cells, *diagonally lined bars* (B, C, and E). Similar results were obtained in three independent experiments. [A color figure can be viewed in the online version, which is available at www.endo.endojournals.org.

LIGHT alone did not generate any TRAP-positive MNC under the conditions in which RANKL-induced OC formation was significantly decreased by osteoprotegerin. Next, to seek further evidence that a signal through HVEM is responsible for osteoclastogenesis, we attempted to compete out membrane-bound HVEM with soluble HVEM (sHVEM). sHVEM significantly reduced the expression of TRAP in WT cells but had no effect in the HVEM-KO cells (Fig. 4E). These results demonstrate that LIGHT/HVEM interaction is a positive regulator of osteoclastogenesis via a signal through HVEM.

Discussion

We have demonstrated a functional role of HVEM in OC. The absence of HVEM decreased RANKL-induced osteoclastogenesis, suggesting that HVEM is a positive regulator of osteoclastogenesis. However, the decreased number of OC in the mutant appeared not to be caused by OC apoptosis. In fact, *in vivo* TUNEL staining showed more WT OC undergoing apoptosis compared with HVEM-KO OC, which was contrary to the *in vitro* results. One potential explanation for these disparate results is that the net effect of HVEM on OC apoptosis *in vivo* represents the balance of its direct antiapoptotic and indirect apoptotic activities in bone marrow environments. HVEM may play dual roles in OC apoptosis, depending on the ligand and receptor engagement, although it has not been determined yet. In T cells, engagement of HVEM with LIGHT induces powerful immune responses, whereas HVEM interaction with B and T lymphocyte negatively regulates them (13). *In vivo*, this indirect apoptotic activity may overcome the direct suppressive activities of HVEM in OC. The number of large OC (>10 nuclei), which are more efficient at bone resorption, was lower than the total number of OC in the mutant, suggesting that HVEM may be involved in the fusion of OC precursors. OC activation was also impaired by a lack of HVEM. These results clearly indicate that HVEM is at least partly responsible for modulating the number and activity of OC.

HVEM was constitutively expressed in BMM and increased at an early stage of RANKL stimulation but was down-regulated afterward. Its ligand, LIGHT, was also constitutively expressed in BMM and was reciprocally expressed compared with HVEM. Because HVEM belongs to the same TNFR family as RANK, we thought it likely that the HVEM/LIGHT interaction induces osteoclastogenesis independently of RANK/RANKL. However, this was not the case, because LIGHT alone did not generate any OC without RANKL under our assay conditions. On the contrary to our finding, Edwards *et al.* (23) has reported that LIGHT alone induces OC formation and bone resorption without RANKL. This discrepancy could be due to the source of the cells or the assay conditions used. Although our data showed that HVEM affects RANKL-induced signaling in OC, it is not certain through which molecule HVEM participates in the RANKL-stimulated pathway. TRAF are cytoplasmic adaptor proteins binding to various receptors of the TNFR family, including RANK and HVEM. The cytoplasmic domain of HVEM interacts with TRAF1, 2, 3, and 5, but not with TRAF6 (12), which is an essential

adaptor molecule in RANKL signaling in osteoclastogenesis (3). However, TRAF3, which serves as a negative regulator of NF-κB, binds both RANK and HVEM (24). It is possible that HVEM reduces the availability of TRAF3 for RANK, consequently resulting in an increased chance of TRAF6 binding to RANK and enhancing osteoclastogenesis. HVEM-KO mice exhibited a significant increase in BMD and BMC at 10 wk of age, suggesting that HVEM plays a critical role in bone remodeling under physiological conditions. Although we cannot exclude the effect of other molecules binding to HVEM or LIGHT in OC, we have demonstrated that sLIGHT increases OC formation and ROS via HVEM. It is possible that the HVEM/LIGHT interaction plays a role in elevated bone loss in the presence of HVEM. The role of HVEM in bone loss has been implicated by several other studies. A blockade of LIGHT reduced disease severity in a collagen-induced arthritis model (25), possibly due to the decreased availability of LIGHT.

RANKL-induced osteoclastogenesis requires the activation of several signaling pathways. RANKL recruits TRAF6 to activate NF-κB (3), which cooperates with activated c-Fos and AP-1, all of which are necessary for NFAT2 induction (26). Once induced, NFAT2 is activated and amplified by Ca^{2+} signaling. HVEM deficiency decreased RANKL-induced NF-κB activation and also reduced the level of $[Ca^{2+}]$i and $[Ca^{2+}]$i oscillation in a sustained manner upon RANKL stimulation. These results explain the decreased expression of NFAT2 both at the mRNA and protein levels in the absence of HVEM. Decreased NF-κB activation due to HVEM deficiency could delay cooperation of NFATc2 and NF-κB for the initial induction of NFAT2 (26). In addition, a lowered Ca^{2+} signal would attenuate autoamplification of NFAT2.

Although it has not yet been clearly elucidated how RANKL-induced ROS affects $[Ca^{2+}]$i oscillation, both increased levels of ROS and spontaneous $[Ca^{2+}]$i oscillation are observed in peroxiredoxin II-deficient BMM, resulting in increased osteoclastogenesis (22). The absence of HVEM attenuated RANKL-induced ROS generation and exogenous sLIGHT elevated it, indicating that the HVEM/LIGHT interaction plays a role in RANKL-induced long-term ROS production. Other work confirms this; although the response was more immediate than ours, each respective ligation of CD40 and TNFR also generates ROS (27, 28) and LIGHT induced ROS production (16). The long lasting generation of ROS could be caused by ROS-induced ROS release (29). Treatment with a general antioxidant, NAC, abolishes the $[Ca^{2+}]$i oscillation and needs to be continuous for inhibition of OC differentiation (22), indicating that a sustained level of ROS is required for $[Ca^{2+}]$i oscillation and, consequently, osteoclastogenesis.

Bone mass is significantly affected by the redox state *in vivo*. Ovariectomy causes oxidative stress, resulting in a decreased level of the thiol antioxidants glutathione and thioredoxin, as well as their regenerative enzymes (30, 31). Antioxidants prevent estrogen deficiency-induced bone loss, whereas drugs to reduce antioxidants induce bone loss (31). Our findings that lack of HVEM in OC reduced OC formation and activity as well as long-term ROS generation *in vitro* and increased bone mass *in vivo* suggest that HVEM may be a mediator of estrogen deficiency-induced bone loss by acting as a redox regulator. This would establish a novel molecular link between ROS and increased bone loss. Estrogen deficiency could induce bone loss by up-regulating HVEM, resulting in elevated OC formation and bone resorption. Further studies to assess whether estrogen deficiency affects HVEM expression are currently underway. Tipping the balance between ROS and antioxidants under pathological conditions causes oxidative stress and results in bone loss. Further studies exploring whether HVEM depletes antioxidants or generates ROS should be conducted. Understanding the role of HVEM in bone loss as a modulator of the redox state could aid in the design of a novel therapy for osteoporosis by the reduction of oxidative stress.

Acknowledgments

We thank Dr. Eung-Kyun Kim and UNIST-Olympus Biomed Imaging Center (UOBC) for providing the fluorescence images.

Address all correspondence and requests for reprints to: Hye-Seon Choi, Department of Biological Sciences, University of Ulsan, Ulsan 680–749, Korea. E-mail: hschoi@mail.ulsan.ac.kr.

This work was supported by Basic Science Research Program through the National Research Foundation of Korea (NRF) funded by the Ministry of Education, Science and Technology (2009-0066232; BRL 2009-0087350).

Disclosure Summary: The authors have nothing to disclose.

References

1. **Suda T, Takahashi N, Udagawa N, Jimi E, Gillespie MT, Martin TJ** 1999 Modulation of osteoclast differentiation and function by the new members of the tumor necrosis factor receptor and ligand families. Endocr Rev 20:345–357
2. **Kong YY, Yoshida H, Sarosi I, Tan HL, Timms E, Capparelli C, Morony S, Oliveira-dos-Santos AJ, Van G, Itie A, Khoo W, Wakeham A, Dunstan CR, Lacey DL, Mak TW, Boyle WJ, Penninger JM** 1999 OPGL is a key regulator of osteoclastogenesis, lymphocyte development and lymph-node organogenesis. Nature 397:315–323
3. **Wong BR, Josien R, Lee SY, Vologodskaia M, Steinman RM, Choi**

Y 1998 The TRAF family of signal transducers mediates NF-kB activation by the TRANCE receptor. J Biol Chem 273:28355–28359

4. **Iotsova V, Caamaño J, Loy J, Yang Y, Lewin A, Bravo R** 1997 Osteopetrosis in mice lacking NF-κB1 and NF-κB2. Nat Med 3:1285–1289
5. **Takayanagi H, Kim S, Koga T, Nishina H, Isshiki M, Yoshida H, Saiura A, Isobe M, Yokochi T, Inoue J, Wagner EF, Mak TW, Kodama T, Taniguchi T** 2002 Induction and activation of the transcription factor NFATc1 (NFAT2) integrate RANKL signaling in terminal differentiation of osteoclasts. Dev Cell 3:889–901
6. **Yang CR, JH Wang, Hsieh SL, Wang SM, Hsu TL, Lin WW** 2004 Decoy receptor 3 (DcR3) induces osteoclast formation from monocyte/macrophage lineage precursor cells. Cell Death Differentiation 11(Suppl):S97–S107
7. **Shin HH, Kim SJ, Lee DS, Choi HS** 2005 The soluble glucocorticoid-induced tumor necrosis factor receptor (sGITR) stimulates osteoclast differentiation induced by receptor activator of NF-κB Ligand (RANKL) in osteoclast cells. Bone 36:832–839
8. **Shin HH, Lee EA, Kim SJ, Kwon BS, Choi HS** 2006 A signal through 4–1BB ligand inhibits receptor for activation of nuclear factor-κB ligand-induced osteoclastogenesis by increasing interferon-beta production. FEBS Lett 580:1601–1606
9. **Shin HH, Lee JE, Lee EA, Kwon BS, Choi HS** 2006 Enhanced osteoclastogenesis in 4–1BB-deficient mice caused by reduced interleukin-10. J Bone Miner Res 21:1907–1912
10. **Yokoyama M, Ukai T, Ayon Haro ER, Kishimoto T, Yoshinaga Y, Hara Y** 2011 Membrane-bound CD40 ligand on T cells from mice injected with lipopolysaccharide accelerates lipopolysaccharide-induced osteoclastogenesis. J Periodontal Res 46:464–474
11. **Montgomery RI, Warner MS, Lum BJ, Spear PG** 1996 Herpes simplex virus 1 entry into cells mediated by a novel member of the TNF/NGF receptor family. Cell 87:427–436
12. **Marsters SA, Ayres TM, Skubatch M, Gray CL, Rothe M, Ashkenazi A** 1997 Herpesvirus entry mediator, a member of the tumor necrosis factor receptor (TNFR) family, interacts with members of the TNFR-associated factor family and activates the transcription-factors NF-κB and AP-1. J Biol Chem 272:14029–14032
13. **Murphy KM, Nelson CA, Sedý JR** 2006 Balancing co-stimulation and inhibition with BTLA and HVEM. Nat Rev Immunol 6:671–681
14. **Tamada K, Shimozaki K, Chapoval AI, Zhai Y, Su J, Chen SF, Hsieh SL, Nagata S, Ni J, Chen L** 2000 LIGHT, a TNF-like molecule, costimulates T cell proliferation and is required for dendritic cell-mediated allogenic T cell response. J Immunol 164:4105–4110
15. **Morel Y, Truneh A, Sweet RW, Olive D, Costello RT** 2001 The TNF superfamily members LIGHT and CD154 (CD40 ligand) costimulate induction of dendritic cell maturation and elicit specific CTL activity. J Immunol 167:2479–2486
16. **Heo SK, Ju SA, Lee SC, Park SM, Choe SY, Kwon B, Kwon BS, Kim BS** 2006 LIGHT enhances the bactericidal activity of human monocytes and neutrophils via HVEM. J Leukoc Biol 79:330–338
17. **Kim WK, Park JS, Sul OJ, Seo JH, Choi BK, Park HY, Latour AM, Koller BH, Kwon BS, Jeong CS** 2011 Role of TNFR-related 2 mediated immune responses in dextran sulfate sodium-induced inflammatory bowel disease. Mol Cells 31:99–104
18. **Lee JE, Shin HH, Lee EA, Phan TV, Choi HS** 2007 Stimulation of osteoclastogenesis by enhanced level of MIP-1α in BALB/c mice. Exp Hematol 35:1100–1108
19. **Jimi E, Akiyama S, Tsurukai T, Okahashi N, Kobayashi K, Udagawa N, Nishihara T, Takahashi N, Suda T** 1999 Osteoclast differentiation factor acts as a multifunctional regulator in murine osteoclast differentiation and function. J Immunol 163:434–442
20. **Fuller K, Kirstein B, Chambers TJ** 2006 Murine osteoclast formation and function: differential regulation by humoral agents. Endocrinology 147:1979–1985
21. **Sheng ZF, Xu K, Ma YL, Liu JH, Dai RC, Zhang YH, Jiang YB, Liao EY** 2009 Zoledronate reverses mandibular bone loss in osteoprotegrin-deficient mice. Osteoporos Int 20:151–159
22. **Kim MS, Yang YM, Son A, Tian YS, Lee SI, Kang SW, Muallem S, Shin DM** 2010 RANKL-mediated reactive oxygen species pathway that induces long lasting Ca^{2+} oscillations essential for osteoclastogenesis. J Biol Chem 285:6913–6921
23. **Edwards JR, Sun SG, Locklin R, Shipman CM, Adamopoulos IE, Athanasou NA, Sabokbar A** 2006 Light, a novel mediator of bone resorption, is elevated in rheumatic arthritis. Arthritis Rheum 54:1451–1462
24. **Hauer J, Püschner S, Ramakrishnan P, Simon U, Bongers M, Federle C, Engelmann H** 2005 TNF receptor (TNFR)-associated factor (TRAF) 3 serves as an inhibitor of TRAF2/5-mediated activation of the noncanonical NF-κB pathway by TRAF-binding TNFRs. Proc Natl Acad Sci USA 102:2874–2879
25. **Fava RA, Notidis E, Hunt J, Szanya V, Ratcliffe N, Ngam-Ek A, De Fougerolles AR, Sprague A, Browning JL** 2003 A role for the lymphotoxin/LIGHT axis in the pathogenesis of murine collagen-induced arthritis. J Immunol 171:115–126
26. **Asagiri M, Sato K, Usami T, Ochi S, Nishina H, Yoshida H, Morita I, Wagner EF, Mak TW, Serfling E, Takayanagi H** 2005 Autoamplification of NFATc1 expression determines its essential role in bone homeostasis. J Exp Med 202:1261–1269
27. **Ha YJ, Lee JR** 2004 Role of TNF receptor-associated factor 3 in the CD40 signaling by production of reactive oxygen species through association with p40phox, a cytosolic subunit of nicotinamide adenine dinucleotide phosphate oxidase. J Immunol 172:231–239
28. **Shen HM, Pervaiz S** 2006 TNF receptor superfamily-induced cell death: redox-dependent execution. FASEB J 20:1589–1598
29. **Zorov DB, Juhaszova M, Sollott SJ** 2006 Mitochondrial ROS-induced ROS release: an update and review. Biochim Biophys Acta 1757:509–517
30. **Lean JM, Davis JT, Fuller K, Jagger CJ, Kirstein B, Partington GA, Urry ZL, Chambers TJ** 2003 A crucial role for thiol antioxidants in estrogen-deficiency bone loss. J Clin Invest 112:915–923
31. **Lean JM, Jagger CJ, Kirstein B, Fuller K, Chambers TJ** 2005 Hydrogen peroxide is essential for estrogen-deficiency bone loss and osteoclast formation. Endocrinology 146:728–735